Transfer learning between Sentinel-1 acquisition modes enhances the few-shot segmentation of natural oil slicks in the Arctic

Julien Vadnais, *Graduate Student Member, IEEE*, Benjamin Aubrey Robson, Christian Haug Eide, Rune Mattingsdal, Malin Johansson, *Member, IEEE*

***Abstract*—Natural seepage is a significant contributor to marine hydrocarbon inputs. Remote and intermittent seeps are difficult to monitor in the field, yet oil slicks can be observed by spaceborne synthetic aperture radar (SAR) because they reduce backscatter, creating potential for automatic mapping. In mapping tasks like segmentation, deep learning models excel, albeit needing large amounts of labeled images. To deal with scarcity of labeled images, transfer learning is an approach commonly used in computer vision, though still underutilized in remote sensing. In the case of oil slicks, differences between Sentinel-1 acquisition modes, such as the interferometric wide (IW) in the North Sea and extra wide (EW) in the Arctic, complicate direct model transfer. Here, we present a use-case where transfer learning enhances the segmentation of natural oil slicks. We used labeled slicks in IW images in the North Sea to pretrain a series of DeepLabv3 and SAM models. These models were then fine-tuned on EW-labeled slicks from two documented Arctic seeps on which we have only limited observations. Our results show clear evidence that transfer learning improves few-shot segmentation, notably in challenging and noisy images. Overall, few studies have addressed transfer learning between SAR acquisition modes. This work contributes to improved monitoring of poorly understood or yet undiscovered hydrocarbon seeps.**

***Index Terms*—Natural seepage, oil slicks, SAR, deep learning, transfer learning, segmentation, DeepLab, SAM**

I. INTRODUCTION

NATURAL seepage is a significant contributor of oil entering marine environments [1], yet the data required to update quantitative estimates of its global scale remain insufficient, especially outside of the U.S. continental shelf [2]. Because of difficulties in continuously monitoring remote offshore areas, data scarcity has restrained our possibilities of studying the ecosystem contribution and the behavior of hydrocarbon seeps. Synthetic aperture radar (SAR) is well suited to this task due to its capacity to operate in any lighting conditions, and its fine spatial resolution for its wide swath. Surface oil slicks are visible in SAR images because they return lower backscatter compared to surrounding waters, due to the oil damping sea roughness [3]–[5]. Precisely, SAR's capacity for detecting a slick relies on the damping ratio, the contrast in backscatter between oil- and oil-free pixels [6], [7].

Previous works have attempted to make use of the damping ratio for automatizing marine oil detection, with varying results. They face a common challenge which has been an ongoing topic of research for over three decades: the presence of oil look-alikes including ocean eddies, biogenic slicks and newly-formed ice [5], [6], [8], [9]. When trained with a large number of labeled examples, deep learning models, currently the benchmark in computer vision, can capture complex shape- and texture-related features for image classification or segmentation tasks [10]. When trained with a limited sample size, however, these models struggle to extract more abstract, higher-level features [11]. The issue of limited data is exacerbated in the case of oil slicks because of limited visibility. Not only will slicks only last a few hours on the surface [12]–[14], their visibility also depend on a specific window of surface wind conditions, outside of which the sea either has too many or too few capillary waves for a discriminative damping ratio [7], [15], [16]. Slick events are also highly intermittent. Seepage rates vary across both monthly and yearly timescales, and most active seeps have an occurrence rate below 10% [14], [17]. Some seeps remain dormant for months, or even years, before emitting oil again. In two distinct regions, studies found that only half of all seeps show activity at a given time [12], [18], and dormant seeps' occurrence might be underestimated, considering that they are less likely to be discovered.

In this paper, we assess the potential of transfer learning for enhancing automatic mapping of natural oil slicks. Transfer learning, or deep transfer learning in the case of deep learning, aims at transferring valuable and generalizable features from one model to another, where contexts are similar but the target distributions differ [10]. We pretrained two image segmentation models using oil slicks mapped in Sentinel-1 images over the North Sea. These models were then fine-tuned on two known seeps in the Arctic, for which we have only limited observations. In the Arctic, Sentinel-1 scenes are mostly acquired in the extra wide (EW) mode at a 25-m pixel spacing with dual HH/HV polarization. However, elsewhere, oil mapping with Sentinel-1 more commonly uses the interferometric wide (IW) mode at a 10-m pixel spacing with VV/VH polarization, as it is the standard mode in oceans outside of polar regions. Little work, if any, has addressed transfer learning between SAR acquisition modes, and we believe natural oil slicks make a prime example of a real-life application of deep-learning mapping with few labeled data.

Manuscript received March 4, 2025. This research was carried out in the context of the InFluSe project (Research Council of Norway Project 353044).

Julien Vadnais, Benjamin Aubrey Robson, and Christian Haug Eide are with the Department of Earth Science, University of Bergen, 5020 Bergen, Norway. Rune Mattingsdal is with the Norwegian Offshore Directorate, 9406 Harstad, Norway. Malin Johansson is with the Department of Physics and Technology, UiT The Arctic University of Norway, 9037 Tromsø, Norway.

Corresponding author email address: julien.vadnais@uib.no. The entire data and code used in this study is accessible on the GitHub repository at https://github.com/julvad/transfer_learning_S1_slicks_arctic

TABLE I
LABELED SLICKS IN THE SOURCE AND TARGET DOMAINS

	Source domain	Target domain	
Sentinel-1 mode/pol.	IW / VV	EW / HH	
Area	North Sea	Svalbard	Barents Sea
Number of images	463	70	88
Period	2017-2021	2015-2024	2015-2020
Number of slicks	~ 1723	~ 81	~ 250

II. DATA AND METHODS

A. Data

Traditional transfer learning in remote sensing imply that the *target domain* D_T and the *source domain* D_S have similar probability distributions between a common raster band $\mathbf{x_i}$ and a common label $\mathbf{y_i}$ [19]. Deep transfer learning is more robust to distribution shifts and can even handle different target classes, yet, this often requires training on massive datasets (e.g. [20], [21]). Our approach is rather a targeted form of deep transfer learning, with a D_S dataset of smaller size, but closer to the D_T. We will now introduce those two domains.

Researchers recently documented two seepage areas in the Norwegian waters. First, [22] investigated an intermittent seeping point west of the Svalbard archipelago (10.42°E, 78.49°N). At this location, we manually delineated 81 slicks in 70 images taken between 2015 and 2024. Second, [23], [24] found extensive evidence of a wide seepage area in the Barents Sea (31.33-32.37°E, 75.15°N-75.35°N). This area is part of Sentralbanken high, a geological structure with prospective hydrocarbon potential, although it remains largely unexplored [25]. There, we delineated 250 slicks in 88 images taken between 2015 and 2020. At these two locations, labeled samples from the horizontal co-polarization (HH) band of Sentinel-1 EW images constitute the D_T (Fig. 1a, 1b). At lower latitudes, various kinds of oil slicks can be observed in the North Sea, a hydrocarbon-rich and seepage-active region [26]. With the same procedure, we delineated over 1700 slicks, this time using the vertical co-polarization (VV) band of 463 Sentinel-1 IW images. Labeled samples in the North Sea constitute the D_S (Fig. 1c). In this study, only the co-polarization bands were used because of their oil-discrimination capacity [3], [27], [28]. Since slicks can be split into segments, we give slick numbers in Table I as approximations only.

Transfer learning of remote sensing imagery requires data alignment [19]. To deal with shape distortion, particularly at higher latitudes, we reprojected all Sentinel-1 scenes into their corresponding UTM zone. This corresponds to the 31N zone for the North Sea, the 32N zone offshore Svalbard, and the 36N zone in the Barents Sea. Because the pixel spacing of EW scenes is 25 m, compared to 10 m for IW scenes, we ran a bilinear interpolation to align the spatial resolutions. A bilinear interpolation is generally preferred when working with continuous raster values such as the SAR backscatter intensity [29]. In the D_T, 30 out of the 158 annotated Sentinel-1 EW HH scenes were retained for the test split—about 19%—and 10% of the training samples were used for validation. We extracted four combinations of square raster tiles, using a tile width of either 256 or 512 pixels, and either downsampling resolution to 25 m or upsampling to 10 m. Contrast normalization is another important preprocessing step, which needs to be robust to outliers [10], [29]. Here, we applied a linear stretch of two standard deviations on clipped tiles, normalizing values over the 8 bit range (0,255):

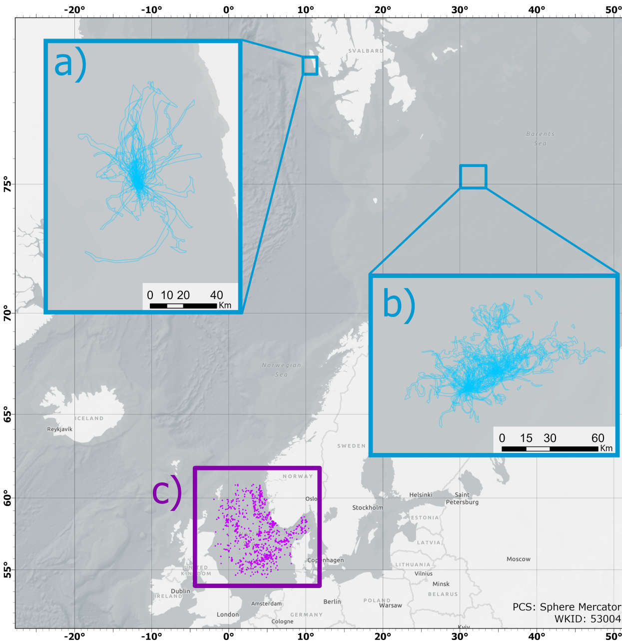

Fig. 1. a) Target domain D_T: Mapped slicks offshore Svalbard
b) Target domain D_T: Mapped slicks in Sentralbanken high, Barents Sea
c) Source domain D_S: Mapped slicks in the North Sea

$$X' = \frac{X - \mu}{2 \cdot \sigma} \cdot 255 \tag{1}$$

in which X' is the new value of image pixels X, using the mean μ and the standard deviation σ of the image.

B. Methods

We pretrained two deep learning models: DeepLabv3 and the Segment Anything Model (SAM). DeepLabv3 is a convolutional neural network architecture for semantic segmentation, which uses atrous convolutions and introduced atrous spatial pooling layers [30]. It is considered state-of-the-art in many fields of application including remote sensing [31]. SAM is a novel zero-shot learning vision transformer for image segmentation [21]. While SAM itself does not assign classes, the SamLoRA variation extends its use by adding trainable classification layers to SAM's mask encoder [32]. Data augmentation was generated in the form of a 30° rotation, brightness and contrast shifts, soft zooms, and croppings. We trained models with two backbones to investigate if a deep or a shallow model would perform best. For DeepLabv3, we used the ResNet-50 and ResNet-101 backbones [20]; ViT-B and ViT-L checkpoints were used for SAM [21]. The learning rate was determined from a pretraining learning curve [33], [34]. We used a training batch size of 64 for the 256x256 tiles, and 16 for the 512x512 tiles. Model inference was performed

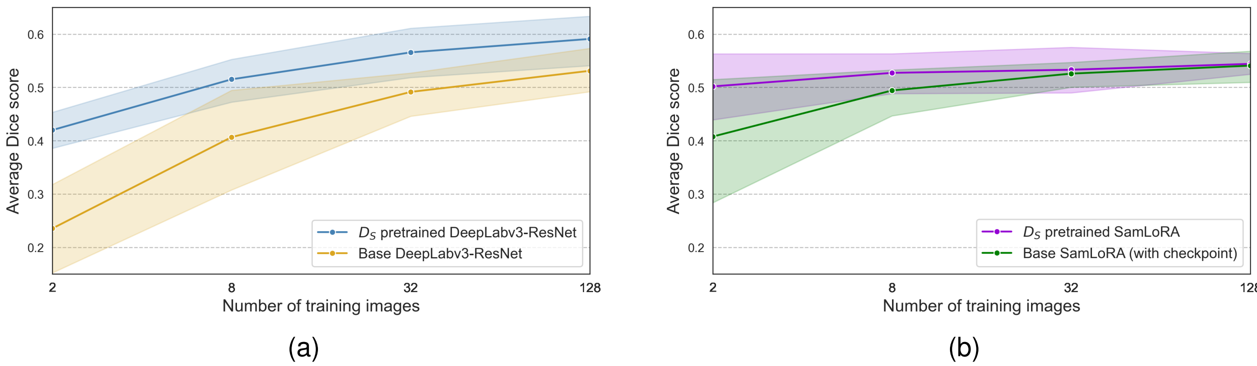

Fig. 2. Average test-set Dice score with 95% statistical interval, depending on the number of training images. (a) DeepLabv3 (b) SamLoRA

in Python using ArcPy and PyTorch, with an RTX 4500 Ada Generation GPU.

We first experimented by training with a weighted binary cross-entropy loss function, defined by:

$$L_{CE} = -\frac{w}{N}\sum_{i=1}^{N}\left[y_i \log(\hat{y}_i) + (1-y_i)\log(1-\hat{y}_i)\right] \quad (2)$$

Here, y_i represents the ground truth label (0: water; 1: slick) and $\hat{y}_i$ is the softmax predicted value of the i-th pixel. This function introduces w, a weight parameter calculated as a scalar inversely proportional to slick pixel frequency [35]. To further handle the frequency imbalance between oil and water pixels, we added a term based on the loss function from [36] (L_{Dice}), resulting in the Dice-weighted function:

$$L = (1-\alpha) \cdot L_{CE} + \alpha \cdot L_{\text{Dice}} \quad (3)$$

where α is a float between 0 and 1, a tunable hyperparameter indicating the Dice loss fraction. With α set to 0.5, as in [37], this Dice-weighted function (L) proved the most effective during preliminary tests.

Using all 463 images from the D_S, we pretrained models for a maximum of 100 epochs with validation-loss early-stopping as a means of limiting overfitting [38]. We then generated 8 bootstrapped sets for each value in the set $N = \{2, 8, 32, 128\}$, where N is the number of training images from the D_T. No bootstrapping was done at $N = 128$ as the entire training split was in use. We compared *base models*, which used default backbone weights, and *fine-tuned models*, which were instead initialized with full weights from the model pretrained on the D_S. These weights are left unfrozen in the D_T fine-tuning stage [39]. We calculated the Dice score for a total of 128 models on the test split, considering only the oil slick class to ignore the trivial classification of water. The Dice score, closely related to the F1, is calculated as:

$$\text{Dice} = \frac{2 \cdot TP}{2 \cdot TP + FP + FN} \quad (4)$$

Bootstrapped testing helps assess model consistency with small and high-variance test sets [40]. In Fig. 2 and Table II, we provide a 95% statistical interval for the test-set Dice score, following the bootstrapping method described in [41].

TABLE II
AVERAGE DICE AND CHANGE OBSERVED WITH TRANSFER LEARNING, BASED ON THE SPATIAL ALIGNMENT METHOD

Tile size	25 m downsampling	10 m upsampling
256x256	$0.49(+0.13 \pm 0.13)$	$0.49(+0.05 \pm 0.04)$
512x512	$0.42(+0.11 \pm 0.28)$	$0.51(+0.03 \pm 0.05)$

III. RESULTS AND DISCUSSION

Fig. 2 illustrates the change in Dice score as the number of training images increases. We show clear evidence that both the convolutional neural network (Fig. 2a) and the vision transformer (Fig. 2b) benefit from transfer learning. This result is more evident in the case of DeepLabv3, in which D_S pretraining increased the Dice score at all values of N. While SamLoRA also benefits, the effect is rapidly reduced as the number of training samples grow, and its effect is indistinguishable with values of $N > 8$. Despite this, transfer learning has an overall positive effect, particularly with fewer training images. Until $N > 8$, SamLoRA outperforms DeepLabv3. This is consistent with larger models being more efficient at fine-tuning on a small number of samples [42]. DeepLabv3's Dice scores grow steadily with an increasing number of training images, and we can expect this trend to continue beyond the limits of our sample size (Fig. 2a). In contrast, it remains unclear whether SamLoRA would benefit from transfer learning with larger training datasets (Fig. 2b).

After comparing model architectures, we investigated the effect of transfer learning depending on the resampling method used to geographically align images from two Sentinel-1 acquisition modes. Table II compares these methods, presenting the average Dice score accompanied by a 95% statistical interval for the change in Dice resulting from transfer learning. In most cases, transfer learning improves model performance, but its effect is strongest—yet highly variable—when downsampling images to 25 m, meaning that we align the D_S IW images with the D_T EW images. Similar work by [43] found that fine-tuning improved deep learning segmentation of oil spills. In that study, however, the researchers downsampled the resolution of training images to create a synthetic pretraining dataset. Moreover, tile size has no apparent effect on transfer learning. This is an interesting finding, because large

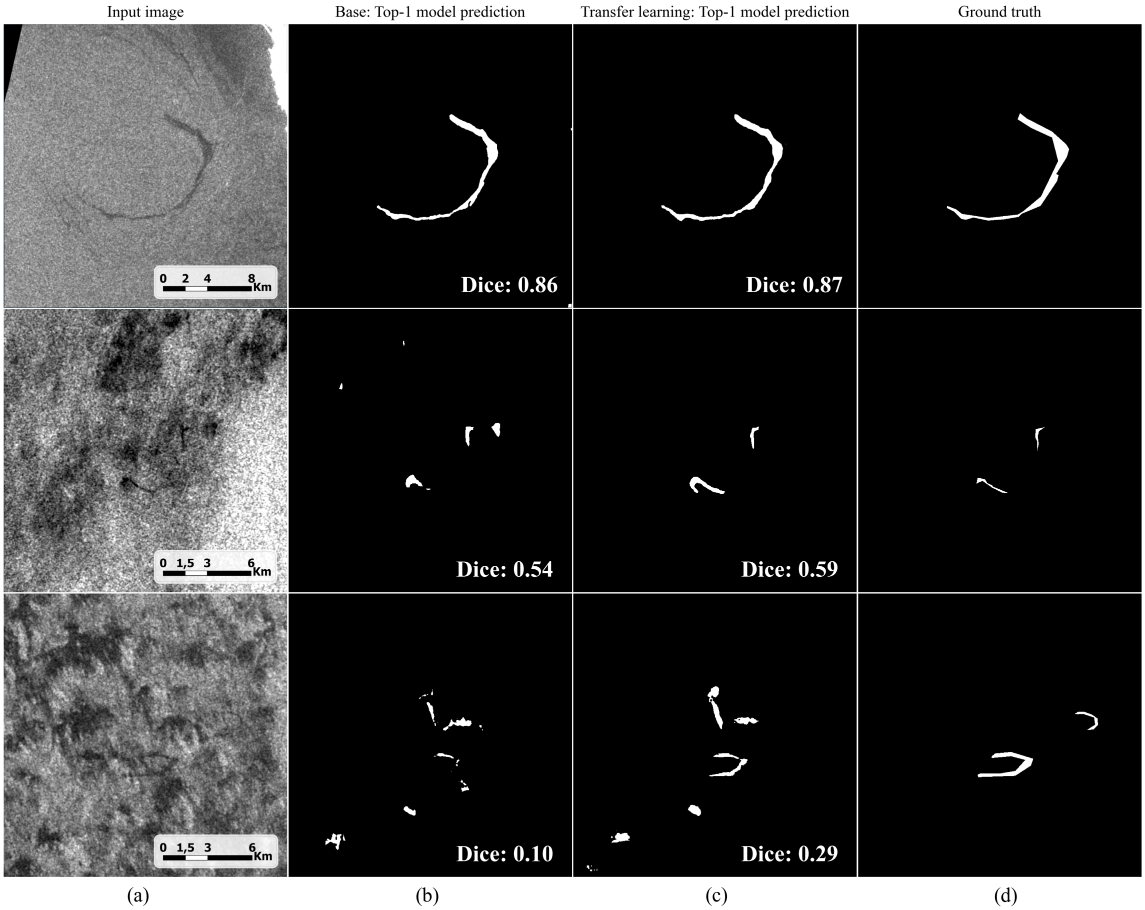

Fig. 3. Top-1 model performance through examples. Top row: An easier case, with some ocean eddies. Middle: A more challenging example with various look-alike features. Bottom: Arguably one of the most challenging cases. A small, low-contrast slick is missed by models in the center right of the image.

geophysical processes, such as oil slicks, often need to be split into smaller tiles for processing. This typically results in performance loss and slower computing.

Fig. 3 displays the segmentation predictions from the top-performing model (Top-1). We compare predictions from the base (Fig. 3b) and the fine-tuned (Fig. 3c) versions, showing how the model benefited from transfer learning across different examples. The examples are taken from the test set, with a 25 m resolution and predicting with a tile width of 512 pixels, the most challenging format evaluated (Table II). First, we see a typical arc-shaped slick with a clear SAR damping ratio (top, Fig. 3a). Both the base and the fine-tuned model delineate the slick, while correctly leaving out ocean eddies and a low-wind area on top of the image. The second row presents a common appearance of natural slicks in an SAR image, where several dark features may trigger false detections (middle, Fig. 3a). Nonetheless, both models detect the two slicks (middle, Fig. 3d) and transfer learning help reduce false detections, despite a somewhat undervalued Dice score (middle, Fig. 3c). The last row (bottom, Fig. 3a) exemplifies one of the most challenging cases for SAR slick mapping. If two low-contrast slicks can be seen among look-alike features, only the main slick (bottom, Fig. 3d) is detected by the fine-tuned model (bottom, Fig. 3c), illustrating the challenge of harsh mapping conditions.

IV. Conclusion

Applications of transfer learning must be carefully evaluated. In many cases, its use can be inefficient, even detrimental, if the contexts are too different [44]. In this study, we made use of labeled slicks from a different area and imaged in a different SAR acquisition mode. We show that transfer learning in the form of fine-tuning is effective for the few-shot SAR segmentation of natural oil slicks, improving model performance (average Dice increase of 0.03–0.13) despite accessing only a few examples in the target domain.

Transferability between IW and EW modes is especially important in the Arctic, where the absence of large spills–which oil segmentation models typically rely on for training–limits the availability of training data. In contrast, Arctic seeps emit slicks that are typically thin, with low oil concentrations and reduced backscatter damping. This poses a challenge for detection, which partly explains why these remote seeps are still under-investigated today. Our results show that both deep learning models benefited from transferring pretrained model weights, with DeepLabv3 performing best overall, though SAM achieved top accuracy with fewer training images. Our method, validated on two documented seepage sites, offers promising perspectives for identifying and studying additional, as yet undiscovered remote seeps.

Acknowledgments

Julien Vadnais received financial support from the Doctoral Research Scholarship of the Fonds de recherche du Québec. The authors would like to thank the EU Copernicus programme for allowing open access to the Sentinel-1 archives. This research was carried out as part of the InFluSe project (Research Council of Norway Project 353044).

References

[1] K. A. Kvenvolden and C. K. Cooper, "Natural seepage of crude oil into the marine environment," *Geo-Marine Letters*, vol. 23, no. 3, pp. 140–146, Dec. 2003.

[2] National Academies of Sciences, Engineering, and Medicine, *Oil in the Sea IV: Inputs, Fates, and Effects*. Washington, D.C.: National Academies Press, Dec. 2022.

[3] C. Brekke and C. E. Jones, "SAR oil spill imaging, interpretation and information retrieval techniques," in *Maritime Surveillance with Synthetic Aperture Radar*. IET Digital Library, Nov. 2020, pp. 227–267.

[4] M. Fingas and C. E. Brown, "A Review of Oil Spill Remote Sensing," *Sensors*, vol. 18, no. 1, p. 91, Jan. 2018.

[5] W. Alpers and H. A. Espedal, "Oils and surfactants," *Synthetic aperture radar marine user's manual*, pp. 263–275, 2004.

[6] H. Hovland, J. Johannessen, and G. Digranes, "Slick detection in SAR images," in *Proceedings of IGARSS '94 - 1994 IEEE International Geoscience and Remote Sensing Symposium*, vol. 4, Aug. 1994.

[7] C. Quigley, A. M. Johansson, and C. E. Jones, "An Investigation on the Damping Ratio of Marine Oil Slicks in Synthetic Aperture Radar Imagery," *IEEE Journal of Selected Topics in Applied Earth Observations and Remote Sensing*, vol. 16, pp. 5488–5501, 2023.

[8] A. M. Johansson, M. M. Espeseth, C. Brekke, and B. Holt, "Can Mineral Oil Slicks Be Distinguished From Newly Formed Sea Ice Using Synthetic Aperture Radar?" *IEEE Journal of Selected Topics in Applied Earth Observations and Remote Sensing*, vol. 13, pp. 4996–5010, 2020.

[9] W. Alpers, B. Holt, and K. Zeng, "Oil spill detection by imaging radars: Challenges and pitfalls," *Remote sensing of environment*, vol. 201, pp. 133–147, 2017.

[10] I. Goodfellow, Y. Bengio, A. Courville, and Y. Bengio, *Deep Learning*. MIT press Cambridge, 2016, vol. 1.

[11] Y. Bengio, "Deep Learning of Representations for Unsupervised and Transfer Learning," in *Proceedings of ICML Workshop on Unsupervised and Transfer Learning*, Jun. 2012, pp. 17–36.

[12] R. Jatiault, D. Dhont, L. Loncke, and D. Dubucq, "Monitoring of natural oil seepage in the Lower Congo Basin using SAR observations," *Remote Sensing of Environment*, vol. 191, pp. 258–272, Mar. 2017.

[13] S. Daneshgar Asl, D. S. Dukhovskoy, M. Bourassa, and I. R. MacDonald, "Hindcast modeling of oil slick persistence from natural seeps," *Remote Sensing of Environment*, vol. 189, pp. 96–107, Feb. 2017.

[14] C. O'Reilly, M. Silva, S. Daneshgar Asl, W. P. Meurer, and I. R. MacDonald, "Distribution, Magnitude, and Variability of Natural Oil Seeps in the Gulf of Mexico," *Remote Sensing*, vol. 14, no. 13, 2022.

[15] B. A. Saus, "Detection and Delineation of Produced Water Slicks in Sentinel-1 Synthetic Aperture Radar Images," Master's thesis, UiT The Arctic University of Norway, Jun. 2021.

[16] M. Gade, W. Alpers, H. Hühnerfuss, H. Masuko, and T. Kobayashi, "Imaging of biogenic and anthropogenic ocean surface films by the multifrequency/multipolarization SIR-C/X-SAR," *Journal of Geophysical Research: Oceans*, vol. 103, no. C9, pp. 18 851–18 866, 1998.

[17] R. Jatiault, P. Henry, L. Loncke, M. Sadaoui, and D. Sakellariou, "Natural oil seep systems in the Aegean Sea," *Marine and Petroleum Geology*, vol. 163, p. 106754, May 2024.

[18] O. Garcia-Pineda, I. MacDonald, B. Zimmer, B. Shedd, and H. Roberts, "Remote-sensing evaluation of geophysical anomaly sites in the outer continental slope, northern Gulf of Mexico," *Deep Sea Research Part II: Topical Studies in Oceanography*, vol. 57, 2010.

[19] D. Tuia, C. Persello, and L. Bruzzone, "Domain Adaptation for the Classification of Remote Sensing Data: An Overview of Recent Advances," *IEEE Geoscience and Remote Sensing Magazine*, vol. 4, no. 2, pp. 41–57, 2016.

[20] K. He, X. Zhang, S. Ren, and J. Sun, "Deep Residual Learning for Image Recognition," Dec. 2015.

[21] A. Kirillov, E. Mintun, N. Ravi, H. Mao, C. Rolland, L. Gustafson, T. Xiao, S. Whitehead, A. C. Berg, W.-Y. Lo, P. Dollár, and R. Girshick, "Segment Anything," Apr. 2023.

[22] G. Panieri, C. Argentino, S. P. Ramalho, F. Vulcano, A. Savini, L. Fallati, T. Brekke, G. Galimberti, F. Riva, J. Balsa, M. H. Eilertsen, R. Stokke, I. H. Steen, D. Sahy, D. Kalenitchenko, S. Büenz, and R. Mattingsdal, "An Arctic natural oil seep investigated from space to the seafloor," *Science of The Total Environment*, vol. 907, Jan. 2024.

[23] P. Serov, R. Mattingsdal, M. Winsborrow, H. Patton, and K. Andreassen, "Widespread natural methane and oil leakage from sub-marine Arctic reservoirs," *Nature Communications*, vol. 14, no. 1, p. 1782, Mar. 2023.

[24] A. Yu. Ivanov, E. R. Matrosova, A. Yu. Kucheiko, N. A. Filimonova, N. V. Evtushenko, N. V. Terleeva, and N. V. Libina, "Search and Detection of Natural Oil Seeps in the Seas Surrounding the Russian Federation Using Spaceborne SAR Imagery," *Izvestiya, Atmospheric and Oceanic Physics*, vol. 56, no. 12, pp. 1590–1604, Dec. 2020.

[25] B. A. Lundschien, R. Mattingsdal, S. K. Johansen, and S.-M. Knutsen, "North Barents Composite Tectono-Sedimentary Element," *Geological Society, London, Memoirs*, vol. 57, no. 1, pp. M57–2021–39, Oct. 2025.

[26] M. Hovland and A. G. Judd, "Chapter 2: Focus on North Sea Pockmarks," in *Seabed Pockmarks and Seepages: Impact on Geology, Biology and the Marine Environment*. London: Graham and Trotman Limited, 1988, pp. 8–34.

[27] V. N. Kudryavtsev, B. Chapron, A. G. Myasoedov, F. Collard, and J. A. Johannessen, "On Dual Co-Polarized SAR Measurements of the Ocean Surface," *IEEE Geoscience and Remote Sensing Letters*, vol. 10, no. 4, pp. 761–765, Jul. 2013.

[28] A. M. Johansson, C. Brekke, and G. Spreen, "Multi-frequency polarimetric SAR signatures of lead sea ice and oil spills," in *2017 IEEE International Geoscience and Remote Sensing Symposium (IGARSS)*, Jul. 2017, pp. 1872–1875.

[29] R. A. Schowengerdt, *Remote Sensing: Models and Methods for Image Processing*. Elsevier, Aug. 2006.

[30] L.-C. Chen, G. Papandreou, I. Kokkinos, K. Murphy, and A. L. Yuille, "DeepLab: Semantic Image Segmentation with Deep Convolutional Nets, Atrous Convolution, and Fully Connected CRFs," *IEEE Transactions on Pattern Analysis and Machine Intelligence*, vol. 40, no. 4, pp. 834–848, Apr. 2018.

[31] D. Tuia, D. Marcos, K. Schindler, and B. Le Saux, "Deep Learning-based Semantic Segmentation in Remote Sensing," in *Deep Learning for the Earth Sciences*, 1st ed., G. Camps-Valls, D. Tuia, X. X. Zhu, and M. Reichstein, Eds. Wiley, Sep. 2021, pp. 46–66.

[32] Esri, "Finetune Segment Anything Model (SAM) using SamLoRA," https://developers.arcgis.com/python/latest/guide/finetune-sam-using-samlora/, 2025.

[33] L. N. Smith, "Cyclical Learning Rates for Training Neural Networks," in *2017 IEEE Winter Conference on Applications of Computer Vision (WACV)*, Mar. 2017, pp. 464–472.

[34] J. Howard and S. Gugger, "Fastai: A Layered API for Deep Learning," *Information*, vol. 11, no. 2, p. 108, Feb. 2020.

[35] R. Azad, M. Heidary, K. Yilmaz, M. Hüttemann, S. Karimijafarbigloo, Y. Wu, A. Schmeink, and D. Merhof, "Loss functions in the era of semantic segmentation: A survey and outlook," *arXiv preprint arXiv:2312.05391*, 2023.

[36] F. Milletari, N. Navab, and S.-A. Ahmadi, "V-Net: Fully Convolutional Neural Networks for Volumetric Medical Image Segmentation," in *2016 Fourth International Conference on 3D Vision*, 2016, pp. 565–571.

[37] S. A. Taghanaki, Y. Zheng, S. Kevin Zhou, B. Georgescu, P. Sharma, D. Xu, D. Comaniciu, and G. Hamarneh, "Combo loss: Handling input and output imbalance in multi-organ segmentation," *Computerized Medical Imaging and Graphics*, vol. 75, pp. 24–33, Jul. 2019.

[38] Y. Wang, Q. Yao, J. T. Kwok, and L. M. Ni, "Generalizing from a Few Examples: A Survey on Few-shot Learning," *ACM Comput. Surv.*, vol. 53, no. 3, pp. 63:1–63:34, Jun. 2020.

[39] J. Yosinski, J. Clune, Y. Bengio, and H. Lipson, "How transferable are features in deep neural networks?" in *Advances in Neural Information Processing Systems*, vol. 27. Curran Associates, Inc., 2014.

[40] K. Møllersen and E. Holsbø, "Accounting for multiplicity in machine learning benchmark performance," Sep. 2024.

[41] A. Burkov, *Machine Learning Engineering*. True Positive, Sep. 2020.

[42] X. Zhai, A. Kolesnikov, N. Houlsby, and L. Beyer, "Scaling Vision Transformers," in *Proceedings of the IEEE/CVF Conference on Computer Vision and Pattern Recognition*, 2022, pp. 12 104–12 113.

[43] F. M. Bianchi, M. M. Espeseth, and N. Borch, "Large-Scale Detection and Categorization of Oil Spills from SAR Images with Deep Learning," *Remote Sensing*, vol. 12, no. 14, p. 2260, Jan. 2020.

[44] T. Mensink, J. Uijlings, A. Kuznetsova, M. Gygli, and V. Ferrari, "Factors of Influence for Transfer Learning Across Diverse Appearance Domains and Task Types," *IEEE Transactions on Pattern Analysis and Machine Intelligence*, vol. 44, no. 12, pp. 9298–9314, Dec. 2022.